

1 **Arctic-wide sea ice thickness estimates from combining**  
2 **satellite remote sensing data and a dynamic ice-ocean**  
3 **model with data assimilation during the CryoSat-2**  
4 **period**

5 **Longjiang Mu<sup>1,2</sup>, Martin Losch<sup>2</sup>, Qinghua Yang<sup>1</sup>, Robert Ricker<sup>2</sup>, Svetlana N.**  
6 **Losa<sup>2,3</sup>, and Lars Nerger<sup>2</sup>**

7 <sup>1</sup>Guangdong Province Key Laboratory for Climate Change and Natural Disaster Studies, and School of  
8 Atmospheric Sciences, Sun Yat-sen University, Zhuhai, China

9 <sup>2</sup>Alfred Wegener Institute, Helmholtz Centre for Polar and Marine Research, Bremerhaven, Germany

10 <sup>3</sup>Shirshov Institute of Oceanology, Russian Academy of Sciences, Moscow, Russia

11 **Key Points:**

- 12 • A new Arctic sea ice thickness record is generated by assimilating CryoSat-2 and  
13 SMOS thickness products simultaneously.
- 14 • The new sea ice thickness data are close to satellite data in freezing seasons and  
15 further cover the summer seasons.
- 16 • Comparisons with in-situ observations show the new record has some advantages  
17 over PIOMAS and CS2SMOS thickness.

---

Corresponding author: Qinghua Yang, yangqh25@mail.sysu.edu.cn

**Abstract**

Exploiting the complementary character of CryoSat-2 and Soil Moisture and Ocean Salinity (SMOS) satellite sea ice thickness products, daily Arctic sea ice thickness estimates from October 2010 to December 2016 are generated by an Arctic regional ice-ocean model with satellite thickness assimilated. The assimilation is performed by a Local Error Subspace Transform Kalman filter (LESTKF) coded in the Parallel Data Assimilation Framework (PDAF). The new estimates can be generally thought of as combined model and satellite thickness (CMST). It combines the skill of satellite thickness assimilation in the freezing season with the model skill in the melting season, when neither CryoSat-2 nor SMOS sea ice thickness is available. Comparisons with in-situ observations from the Beaufort Gyre Exploration Project (BGEP), Ice Mass Balance (IMB) Buoys and the NASA Operation IceBridge demonstrate that CMST reproduces most of the observed temporal and spatial variations. Results also show that CMST compares favorably to the Pan-Arctic Ice Ocean Modeling and Assimilation System (PIOMAS) product, and even appears to correct known thickness biases in PIOMAS. Due to imperfect parameterizations in the sea ice model and satellite thickness retrievals, CMST does not reproduce the heavily deformed and ridged sea ice along the northern coast of the Canadian Arctic Archipelago (CAA) and Greenland. With the new Arctic sea ice thickness estimates sea ice volume changes in recent years can be further assessed.

**1 Introduction**

Arctic sea ice extent as an indicator of climate change has been monitored by satellites for decades. On the one hand, the linkages between the Arctic ice extent and mid-latitude climate have been documented several times (Francis et al., 2009; Kumar et al., 2010; Liu et al., 2012; Overland & Wang, 2010; Serreze et al., 2007). On the other hand, sea ice thickness may be a more important observable than extent or concentration because it is more directly related to sea ice volume. It is, however, more difficult to observe from space. The sparsity of thickness data results in an incomplete closure of the surface energy and freshwater budgets in the Arctic Ocean (Haine et al., 2015). There are ongoing efforts to construct consistent time series of Arctic sea ice thickness from satellite remote sensing data. Freeboard measurements by satellite altimeters on the Ice, Cloud, and land Elevation Satellite (ICESat) and CryoSat-2 can be used to obtain sea ice thickness estimates assuming hydrostatic equilibrium (Kwok et al., 2009; Laxon et al., 2013).

50 Thin ice thickness can be retrieved by exploiting the brightness temperature observa-  
51 tions at the L-band frequency of 1.4 GHz from the Soil Moisture Ocean Salinity (SMOS)  
52 satellite (Tian-Kunze et al., 2014). To bridge the gap between ICESat and ICESat-2 (sched-  
53 uled for launch in 2018), the NASA IceBridge airborne campaigns are conducted every  
54 year in spring from 2009 providing valuable information of ice and snow thickness in dif-  
55 ferent regions of the Western Arctic (Kurtz et al., 2013). This airborne data record can  
56 also be used for validation of satellite-derived sea ice thickness.

57 Often, retrieval algorithms result in large uncertainties in derived satellite data prod-  
58 ucts. There are different assumptions for snow loading and empirical parameters as well  
59 as intrinsic limitations of different satellite sensors (radar/laser altimetry, radiometry)  
60 so that there can be large differences between different products (Wang et al., 2016). The  
61 uncertainties of different products also differ depending on the used methods and the prop-  
62 erties of the sensed ice cover. In spite of these uncertainties, satellite data products re-  
63 solve ice thickness changes on basin and regional scales. In addition, uncertainties can  
64 be reduced by combining different ice thickness data products. For example, the com-  
65plementary character of the uncertainties in CryoSat-2 and SMOS ice thickness prod-  
66 ucts makes it possible to combine the data with an optimal interpolation scheme into  
67 a merged product CS2SMOS with better spatial and temporal coverage than the indi-  
68 vidual data sets (Ricker et al., 2017). With this combination the overall uncertainties  
69 in Arctic sea ice thickness can be reduced by implementing the individual advantages  
70 of each product. The CS2SMOS dataset covers the entire Arctic and provides ice thick-  
71 ness and the related uncertainties during the freezing season. The drawbacks of the CS2SMOS  
72 dataset are that the data are not available during the melt season in spring and sum-  
73 mer and that the optimal interpolation method is purely statistical and does not con-  
74 tain any information from physical processes (Mu et al., 2018).

75 For a continuous long-term ice thickness record, numerical model estimates can be  
76 used to fill the gaps in the satellite products, especially during summer. The Pan-Arctic  
77 Ice-Ocean Modeling and Assimilation System (PIOMAS) provides sea ice thickness and  
78 volume records that have been evaluated and tuned with submarine data and ICESat  
79 derived ice thickness (Zhang & Rothrock, 2003; Schweiger et al., 2011). PIOMAS data  
80 have become a reference dataset especially for thickness time series in the Arctic, but  
81 the data appear to overestimate thin ice thickness in the Beaufort Sea and underesti-  
82 mate thick ice around the Canadian Arctic Archipelago (CAA) area compared to Ice-

83 Bridge thickness (Wang et al., 2016). These biases are also found to be generally sys-  
84 tematic within other models (Johnson et al., 2012). Most of state-of-the-art ocean-sea  
85 ice models do not represent landfast ice areas properly. Further, many models have bi-  
86 ases in the ice growth rate especially during the early freezing period (Johnson et al.,  
87 2012). Assimilating sea ice thickness data from satellite-based remote sensing is expected  
88 to reduce these sea ice thickness biases in the model. For example, Lisæter et al. (2007)  
89 showed in idealized experiments with synthetic CryoSat data that sea ice and ocean state  
90 variables improve with sea ice thickness data assimilation. A series of studies also showed  
91 that the assimilation of SMOS ice thickness significantly improves the first-year ice es-  
92 timates (Yang et al., 2014, 2016b; Xie et al., 2016). Assimilating CryoSat-2 ice thick-  
93 ness data in addition to SMOS ice thickness into an ice-ocean model in the cold season  
94 lead to a reliable pan-Arctic sea ice thickness estimate that is consistent with in-situ ob-  
95 servations (Mu et al., 2018) .

96 Both SMOS and CryoSat-2 thickness retrieval algorithms fail in the presence of wa-  
97 ter on the ice, for example in melt ponds, so that these data are restricted to the cold  
98 season. To include the melting season, we extend the study of Mu et al. (2018) to cover  
99 the entire CryoSat-2 period from October 2010 to December 2016. The weekly averaged  
100 CryoSat-2 ice thickness is assimilated into the model using a new Kalman filter (more  
101 details in Section 3.3) in addition to the daily Special Sensor Microwave Imager Sounder  
102 (SSMIS) sea ice concentration and SMOS sea ice thickness data. The sea ice thickness  
103 assimilated in the freezing season is expected to provide a good initial state for sea ice  
104 thickness in the melt season when thickness data are not available (Day et al., 2014). First  
105 results confirm this expectation (Blockley & Peterson, 2018). The assimilated sea ice con-  
106 centration in summer has some potential to correct potential sea ice thickness biases by  
107 means of their covariance (Yang et al., 2015a, 2015b, 2016a). Therefore, the new dataset  
108 is expected to cover the entire Arctic without the temporal gaps in CS2SMOS and with  
109 satellite sea ice thickness information that is not included in PIOMAS.

110 The paper is organized as follows: In section 2, we describe the satellite-based sea  
111 ice thickness observations, model and in-situ measurements that are used for assimila-  
112 tion and evaluation. In section 3, we detail the method to establish our model thickness  
113 estimates. The evaluation metrics and comparisons between different products and in-  
114 situ observations are presented in section 4. The results are discussed in section 5 and  
115 conclusions are drawn in section 6.

## 2 Sea Ice Thickness Data

### 2.1 Soil Moisture Ocean Salinity (SMOS) Thickness Data

The SMOS satellite was launched by the European Space Agency (ESA) in 2009 and provides brightness temperature. A thermodynamic sea ice model and a single-layer emissivity model are used to retrieve ice thickness from the brightness temperature (Tian-Kunze et al., 2014). A daily ice thickness product with a spatial resolution of 12.5 km on the National Snow and Ice Data Center (NSIDC) polar-stereographic grid projection is available at the Integrated Climate Data Center (ICDC) at the University of Hamburg (<http://icdc.cen.uni-hamburg.de/>). Because of the specific assumptions of the retrieval algorithm, data with an uncertainty  $> 1$  m or with a ratio between retrieved and maximum retrievable sea ice thickness near 100% are flagged and not used. In practice, this means that only the SMOS data with thickness  $< 1$  m are used for assimilation.

In this study, the SMOS v3.1 ice thickness data are used covering the period 2010–2016. The daily product also contains uncertainty estimates. These are used as assumed observation errors during the data assimilation. Data and uncertainties are linearly interpolated onto the model grid.

### 2.2 CryoSat-2 Thickness Data

CryoSat-2, also launched by the ESA in 2010, is dedicated to retrieve thickness of perennial sea ice (Wingham et al., 2006). The thickness data are derived from sea ice freeboard data, which are obtained from radar altimeter range measurements. Assuming hydrostatic equilibrium and employing a pragmatic approach on snow loading (Laxon et al., 2013), freeboard can be converted into sea ice thickness. The relative uncertainties are smaller for thick ice than for thin ice because of the relatively larger freeboard of thick ice (Ricker et al., 2014).

Weekly CryoSat-2 ice thickness data from the Alfred Wegener Institute (AWI), Helmholtz Centre for Polar and Marine Research (v1.2) are available for the period 2010–2016 (Ricker et al., 2014, <http://data.meereisportal.de>). This dataset is available on the EASE-Grid 2.0 (Brodzik et al., 2012) with a grid resolution of 25 km. It is then interpolated to our model grid. The uncertainties provided with the data are also used as the assumed

146 observation errors during data assimilation. However, due to the 30 day sub-cycle of CryoSat-  
147 2, weekly means of ice thickness have significant data gaps where orbit coverage is in-  
148 complete.

### 149 **2.3 CS2SMOS**

150 The complementarity of the data coverage as well as the sea ice thickness uncer-  
151 tainties between CryoSat-2 and SMOS inspired a statistically merged product (CS2SMOS)  
152 (Ricker et al., 2017, <http://data.meereisportal.de>). The weekly CS2SMOS sea ice  
153 thickness data cover the entire Arctic including the North Pole and are projected onto  
154 the 25 km EASE-Grid 2.0. Compared to airborne thickness data, CS2SMOS represents  
155 an improvement over CryoSat-2 thickness in the thin ice regimes. CS2SMOS thicknesses  
156 also have a low bias in the mixed first-year and multi-year ice regimes. The uncertain-  
157 ties provided in the dataset can be used to approximate the data error statistics. In this  
158 study, the CS2SMOS v1.3 ice thickness product is used for comparison. The data are  
159 interpolated bi-linearly onto the model grid.

### 160 **2.4 Pan-Arctic Ice Ocean Modeling and Assimilation System (PIOMAS)**

161 The PIOMAS (Zhang & Rothrock, 2003) consists of the Parallel Ocean Program  
162 (POP) and a 12-category thickness and enthalpy distribution sea ice model. The sys-  
163 tem is forced by 10 m surface winds, 2 m surface air temperature, cloud cover, downwelling  
164 longwave radiation, specific humidity, precipitation, evaporation and sea level pressure  
165 from the NCEP/NCAR reanalysis. Sea ice concentration from the NSIDC near-real time  
166 product and sea surface temperature (SST) from the NCEP/NCAR Reanalysis are in-  
167 troduced into the system by nudging and optimal interpolation (Zhang & Rothrock, 2003;  
168 Schweiger et al., 2011). Daily sea ice thickness estimates are provided from 1978 to present  
169 on the PIOMAS grid (<http://psc.ap1.uw.edu/data/>). In this study, the PIOMAS v2.1  
170 ice thickness data set is used for comparison.

### 171 **2.5 Beaufort Gyre Exploration Project (BGEP)**

172 Starting in 2003, the Beaufort Gyre Exploration Project based at the Woods Hole  
173 Oceanographic Institution (BGEP, <http://www.whoi.edu/beaufortgyre>) deploys upward-  
174 looking sonar (ULS) moorings every year at three locations BGEP\_A, BGEP\_B and BGEP\_D

175 (Figure 4). The ULS can measure the ice draft with an error of about 0.1 m (Melling et  
176 al., 1995). Drafts are converted to thickness by multiplying with a factor of 1.1 that is  
177 calculated as the ratio of the mean seawater and sea ice densities (Nguyen et al., 2011).  
178 Note that this draft-thickness conversion is very simple. The uncertainties caused by the  
179 absence of sufficient information about different ice types, ice densities, and snow load-  
180 ing are ignored in the study. In contrast to the IceBridge thickness data (section 2.7),  
181 the BGEF long-term ice thickness observations provide a year-round reference for the  
182 comparisons between different ice thickness products.

## 183 **2.6 Ice Mass Balance (IMB) Buoys**

184 IMB buoys have been deployed for more than two decades and provide a compre-  
185 hensive Lagrangian dataset on sea ice evolution along their drift trajectories (Perovich  
186 et al., 2009, <http://imb-crrel-dartmouth.org>). The acoustic sounder above ice and  
187 the underwater sonar altimeter below ice autonomously measure the ice growth and ab-  
188 lation. The uncertainty of sea ice thickness measured by each acoustic sounder is within  
189 5 mm (Richter-Menge et al., 2006). These long-term (some buoys collected data for nearly  
190 two years) and consistent observations of sea ice thickness support the evaluation of dif-  
191 ferent sea ice thickness products.

192 The deployment positions of IMB buoys are considered strategically for some key  
193 locations or in collocation with other instruments. Note that, generally, IMB buoys tend  
194 to be deployed on thick and level ice floes to achieve the longest possible time series. As  
195 a consequence, comparing the Lagrangian observed thickness and the Eulerian model es-  
196 timates is not entirely consistent and can be ambiguous.

## 197 **2.7 Operation IceBridge**

198 NASA's Operation IceBridge (<https://www.nasa.gov/mission-pages/icebridge/>)  
199 conducts airborne surveys on polar ice in the Arctic and Antarctic. On these flights, a  
200 Snow Radar and the Airborne Topographic Mapper (ATM) onboard the aircraft mon-  
201 itors snow and ice thickness (Kurtz et al., 2013) of ice sheets, ice shelves and sea ice to  
202 bridge the gap between ICESat and ICESat-2 since 2009.

203 We use IceBridge sea ice thickness data from 2011 to 2013 obtained from IceBridge  
204 L4 Sea Ice Freeboard, Snow Depth, and Thickness (IDCSI4) data set, Version 1 (Kurtz

205 et al., 2015, <http://nsidc.org/data/idcsi4>). An experimental Quicklook product of  
 206 IceBridge thickness from 2012 to 2016 are not used because of the potentially larger un-  
 207 certainties. The sea ice thickness data and their uncertainties in IDCSI4 are estimated  
 208 over a 40 m length scale. The IceBridge campaigns for the Arctic conducted during March  
 209 and April provide valuable estimates of approximate maximum ice thickness of the year.

### 210 **3 The Model Sea Ice Thickness Estimates**

#### 211 **3.1 The Arctic Regional Sea Ice-Ocean Model**

212 We use a regional, pan-Arctic sea ice-ocean model (Losch et al., 2010; Nguyen et  
 213 al., 2011; Yang et al., 2014; Mu et al., 2017) based on the Massachusetts Institute of Tech-  
 214 nology general circulation model (MITgcm, Marshall et al., 1997). The sea ice dynam-  
 215 ics use a viscous plastics rheology (Hibler III, 1979; Zhang & Hibler, 1997). The sea ice  
 216 thermodynamics use a one-layer, zero heat capacity formulation (Semtner Jr, 1976; Parkin-  
 217 son & Washington, 1979). The sea ice package in the MITgcm also provides an ice thick-  
 218 ness distribution (ITD) model (Ungermann et al., 2017). We do not use the ITD model  
 219 because the redistribution of the ice thickness in different categories under sea ice thick-  
 220 ness assimilation is not straightforward. Snow thickness is a prognostic variable follow-  
 221 ing Zhang et al. (1998). The model sea ice thickness estimates are grid-cell averaged ice  
 222 thickness. This quantity is also called effective ice thickness (Schweiger et al., 2011). Both  
 223 the ocean and sea ice model are discretized on an Arakawa C grid with a grid spacing  
 224 of 18 km. In the vertical direction, there are 50 unevenly spaced layers in the ocean model  
 225 to resolve the halocline in the Arctic Ocean. The bathymetry is derived from the Na-  
 226 tional Centers for Environmental Information (formerly the National Geophysical Data  
 227 Center (NGDC)) 2-minute gridded elevations/bathymetry for the world (ETOPO2, Smith  
 228 & Sandwell, 1997). A global model (Menemenlis et al., 2008) provides monthly oceanic  
 229 boundary conditions for the regional model. Model parameters for sea ice and ocean were  
 230 optimized by Nguyen et al. (2011) using a Green function method and further tuned in  
 231 this study. The albedos for sea ice are set to 0.75 and 0.56 for dry or wet conditions, and  
 232 those for snow are set to 0.84 and 0.70. Additional important parameters are the lead  
 233 closing parameter  $Ho = 0.6074$  and the sea ice strength parameter  $P^* = 2.264 \times 10^4 \text{ Nm}^{-2}$ .  
 234 The ocean model uses free-slip lateral boundary conditions, while for the sea ice model  
 235 no-slip lateral conditions are applied. For more details of the model configuration the  
 236 reader is referred to Losch et al. (2010) and Nguyen et al. (2011).



### 237 **3.2 Atmospheric Forcing**

238 Following Yang et al. (2015a) and Mu et al. (2018), the atmospheric ensemble fore-  
239 casts of the United Kingdom Met Office (UKMO) Ensemble Prediction System (EPS)  
240 (Bowler et al., 2008) available in the TIGGE archive (<http://tigge.ecmwf.int>) are  
241 used to drive the ice-ocean model. There are 23 ensemble members during 1 January 2010  
242 to 15 July 2014, and 11 ensemble members during 6 November 2014 to 31 December 2016,  
243 because the ensemble of UKMO EPS changed from MOGREPS-15 version 14 (UM ver-  
244 sion 8.3) to MOGREPS-G version 15 (UM version 8.5) with a reduced number of ensem-  
245 ble members but with higher horizontal resolution (from N216 to N400). Unfortunately,  
246 there is no UKMO EPS ensemble during this transition from 16 July 2014 to 5 Novem-  
247 ber 2014. The UKMO EPS uses an Ensemble Transform Kalman Filter (ETKF) and the  
248 scheme of Shutts (2005) to take into account the initial uncertainties and the effect of  
249 model uncertainties (Bowler et al., 2008). The ensemble forecasts have been shown to  
250 effectively represent the atmospheric uncertainties of the forecasting system (Yang et al.,  
251 2015a; Mu et al., 2018).

252 The following 6-hourly variables in each forecast were used to generate the fields  
253 to force the ice-ocean model: 2 m dew point temperature, 2 m temperature, 10 m surface  
254 winds, surface pressure, total cloud cover and total precipitation. There is no precipi-  
255 tation output at 0000 UTC, and an additional redistribution of the accumulated precip-  
256 itation is needed to obtain the 6-hourly mean precipitation required by the model. Other  
257 necessary fields, which are not available in the TIGGE archive, are computed by formu-  
258 las using existing data. The specific humidity is calculated from dew point temperature  
259 and surface pressure following Hess (1959). The downward shortwave radiation is cal-  
260 culated from dew point temperature, cloud and astronomical parameters according to  
261 Parkinson & Washington (1979). The downward longwave radiation is calculated based  
262 on 2 m temperature and cloud cover (Parkinson & Washington, 1979).

### 263 **3.3 Satellite Data Assimilation**

264 The Parallel Data Assimilation Framework (PDAF, Nerger & Hiller, 2013, [http://](http://pdaf.awi.de)  
265 [pdaf.awi.de](http://pdaf.awi.de)) is used for assimilating thickness and concentration data. For the sea ice  
266 thickness, the daily SMOS ice thickness data thinner than 1.0 m and the weekly mean

267 CryoSat-2 ice thickness data are assimilated simultaneously into the model as described  
268 in Mu et al. (2018).

269 The sea ice concentration data for data assimilation were processed at IFREMER  
270 and are provided by ICDC (<http://icdc.cen.uni-hamburg.de/>). The ARTIST Sea  
271 Ice (ASI) algorithm is applied to brightness temperatures measured with the 85 GHz SSM/I  
272 and/or SSM/IS channels (Kaleschke et al., 2001; Spreen et al., 2008). The 85 GHz chan-  
273 nel is subject to the weather conditions. To reduce this influence, a 5-day median filter  
274 is applied to the data before publishing (Kern et al., 2010). The spatial resolution of the  
275 sea ice concentration data is  $12.5 \text{ km} \times 12.5 \text{ km}$  in a polar stereographic projection. Fol-  
276 lowing Yang et al. (2016a, 2016b), a uniform constant value of 0.25 fractional sea ice area  
277 is assumed as observational uncertainties accounting for measurement and representa-  
278 tion errors (Janjić et al., 2017) in the study.

279 A model ensemble (section 3.1) is driven by the atmospheric ensemble data sets  
280 derived from the UKMO ensemble forecasts to generate perturbed model states every  
281 day. The uncertainties in the model caused by parameters and imperfect physical pro-  
282 cesses are not considered explicitly (Shlyueva et al., 2016). A variant of the ensemble Kalman  
283 filter, the local version of Error Subspace Transform Kalman Filter (LESTKF), is ap-  
284 plied in the study. The LESTKF provides consistent projections between the ensemble  
285 space and the error subspace (Nerger et al., 2012), and outperforms the Local Singular  
286 Evolutive Interpolated Kalman filter (LSEIK) that was used in Mu et al. (2018). The  
287 sea ice concentration and the sea ice thickness form the state vector. In each analysis  
288 step, the LESTKF corrects the forecast state vector of each model in the ensemble tak-  
289 ing into account the model uncertainties, which are calculated from the ensemble of model  
290 states, and the uncertainties of sea ice concentration and thickness. During this process,  
291 only satellite observations within a radius of 126 km around each model grid point are  
292 considered. This localization radius has been found optimal in Yang et al. (2014) and  
293 was also used in Mu et al. (2018). For the analysis step, the observations are weighted  
294 with distance from the grid point by a quasi-Gaussian weight function (Gaspari & Cohn,  
295 1999). After the analysis step, the ensemble mean sea ice thickness can be thought of  
296 as combined dynamic model and satellite thickness (CMST) estimates. The reader is re-  
297 ferred to Mu et al. (2018) for more details of the data assimilation procedure.

298 During the period without UKMO ensemble forcing data, the model is forced by  
 299 the UKMO unperturbed forcing. Ensemble inflation, which is not necessary with the en-  
 300 semble forcing, is achieved in the LESTKF with a forgetting factor of 0.97 (Yang et al.,  
 301 2015a).

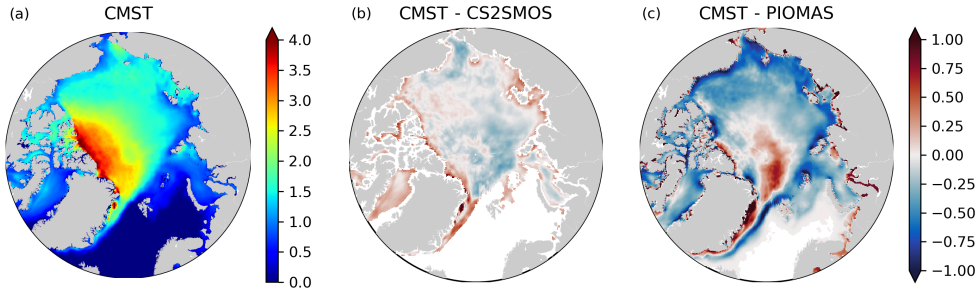
## 302 4 Results

303 We use the root-mean-square deviation (RMSD), the bias and the correlation co-  
 304 efficient as the evaluation metrics for comparing ice thickness data. The RMSD between  
 305 two vectors  $X$  and  $Y$  is calculated as  $\text{RMSD} = \sqrt{E[(X - Y)^2]}$ , the bias ( $B$ ) is calcu-  
 306 lated as  $B = E[X - Y]$ , and the correlation coefficient ( $C$ ) of two vectors is calculated  
 307 as  $C = E[(X - EX)(Y - EY)]/(\sigma_x \sigma_y)$ , where  $E$  is the expectation operator,  $\sigma_x$  and  
 308  $\sigma_y$  are the standard deviations of the vectors  $X$  and  $Y$ , respectively. The centered RMSD  
 309 used for Taylor diagrams is  $\text{CRMSD} = \sqrt{E[((X - EX) - (Y - EY))^2]}$ . The standard  
 310 deviations and the CRMSDs are then normalized by dividing with the standard devi-  
 311 ations of the references, so that  $(\text{CRMSD}/\sigma_{\text{ref}})^2 = (\sigma/\sigma_{\text{ref}})^2 + 1 - 2C\sigma/\sigma_{\text{ref}}$  is always  
 312 satisfied in the Taylor diagrams and all statistics for different references can be shown  
 313 in the same plot. All statistics are calculated over the overlapped temporal and spatial  
 314 coverage for different datasets.

315 Sea ice thickness estimates of each product in section 2 are restricted to the CryoSat-  
 316 2 years 2010 to 2016 for all comparisons. For the comparisons with BGEP ice thickness,  
 317 SMOS, CryoSat-2, CS2SMOS, PIOMAS, and CMST data are interpolated onto the lo-  
 318 cations of the three BGEP moorings. For the comparisons with IMB buoy thickness, the  
 319 above datasets are interpolated onto the daily IMB buoy trajectories. IceBridge thick-  
 320 ness and uncertainties are binned and averaged within each grid cell of our model be-  
 321 fore comparing.

### 322 4.1 Spatial Distribution of Ice Thickness

323 Arctic sea ice volume usually reaches its maximum in April in PIOMAS. Evalu-  
 324 ating the spatial distributions of sea ice thickness during this maximum gives valuable  
 325 insights into the resolved spatial variability of any sea ice product. The SMOS data, how-  
 326 ever, and consequently the CS2SMOS product do not cover the entire April, so that we  
 327 use March sea ice thickness in each dataset for comparison instead.

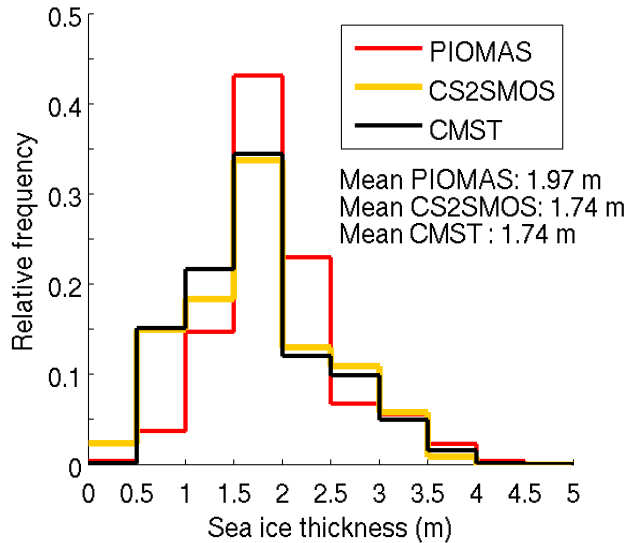


328 **Figure 1.** Comparison of sea ice thickness in March averaged from 2011 to 2016 between  
 329 CMST, CS2SMOS, and PIOMAS. **(a)** CMST sea ice thickness (m) and **(b)** difference (m) be-  
 330 tween CMST and CS2SMOS, and **(c)** difference (m) between CMST and PIOMAS.

331 The March CMST averaged over the years 2011 to 2016 has a thickness below 1.5 m  
 332 along the northern coast of the American Continent and over the Barents Sea, the Kara  
 333 Sea, the Laptev Sea and the Baffin Bay (Figure 1a). The central Arctic is covered by  
 334 thicker ice around 2.0 m with multi-year thick ice above 3.0 m north of the CAA. The  
 335 RMSD of mean March sea ice thickness between CMST and CS2SMOS is 0.16 m (Fig-  
 336 ure 1b). CMST estimates thicker ice (deviations above 0.25 m) in the shallow Siberian  
 337 Seas, north of the CAA and east of Greenland where the uncertainties of CS2SMOS are  
 338 large (Ricker et al., 2017, their Figure 9). The detailed comparisons to in-situ observa-  
 339 tions of sea ice thickness north of the CAA and east of Greenland will be shown in sec-  
 340 tion 4.2.3.

341 March CMST is generally thinner than PIOMAS thicknesses except along the east-  
 342 coast of Greenland, north of Ellesmere Island, and parts of the transpolar drift close to  
 343 Fram Strait (Figure 1c). Differences reach easily 0.5 m in the marginal ice area and in  
 344 the shelf seas. The RMSD between CMST and PIOMAS is 0.41 m. Compared to ICE-  
 345 Sat ice thickness and in-situ ice thickness measurements, PIOMAS tends to overestimate  
 346 the thin ice and underestimate the thick ice (Schweiger et al., 2011). Our results sug-  
 347 gest that our data assimilated model corrects some of these biases present in PIOMAS.

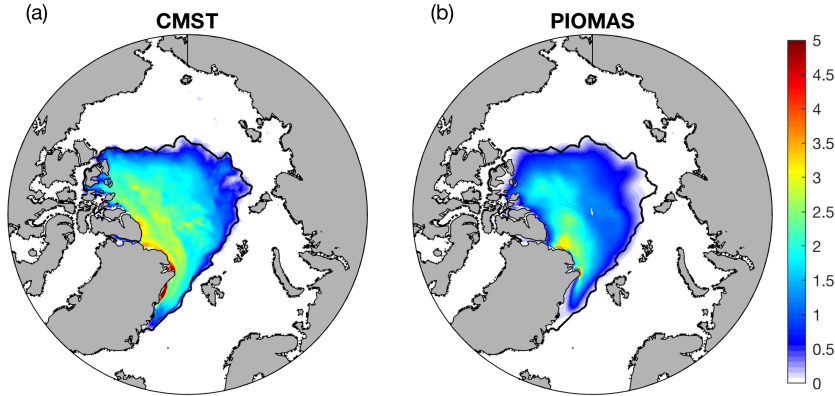
354 The sea ice thickness frequency distributions of the CMST, CS2SMOS, and PIOMAS  
 355 (Figure 2) support this impression. The thickness frequency distributions of CMST and  
 356 CS2SMOS are very similar except for the thinnest category and the 1.0-1.5 m bin. Con-  
 357 sequently the mean thickness of ice north of 65°N is almost exactly the same with 1.74 m



348 **Figure 2.** Histograms of sea ice thickness frequency distributions in March averaged from  
 349 2011 to 2016 for CMST (black), CS2SMOS (orange) and PIOMAS (red). The statistics are  
 350 calculated over the overlapping area of the three datasets.

358 (and equivalently volume of  $13.7 \times 10^3 \text{ km}^3$ ) for CMST and CS2SMOS. The similarity  
 359 of these two estimates is not very surprising, because they both use the same SMOS and  
 360 CryoSat-2 data. In PIOMAS, the mean thickness is 1.97 m and the ice volume is  $15.48 \times$   
 361  $10^3 \text{ km}^3$ . The larger mean thickness is consistent with Figure 1c and also apparent in the  
 362 ice thickness frequency distribution with more ice in thicker categories and less ice in thin-  
 363 ner categories (Figure 2).

364 Climate models tend to underestimate extreme events (Flato et al., 2013), so that  
 365 simulating the record minimum of Arctic sea ice extent in September 2012 represents a  
 366 powerful benchmark test for any sea ice ocean model. The sea ice thickness fields in Septem-  
 367 ber 2012 (Figure 3) of CMST and PIOMAS have similar patterns, but for CMST the  
 368 ice is generally thicker in the central Arctic and along the north coasts of Greenland and  
 369 the CAA. Some of these systematic differences, for example in the central Arctic, can  
 370 already be found in March (not shown, but Figure 1c shows the six-year average). The  
 371 mean thickness, taking into account only ice thicker than 0.05 m, is 1.28 m for CMST and  
 372 0.77 m for PIOMAS. The gradients of sea ice thickness in the marginal ice area (Figure 3)  
 373 are larger in CMST than in PIOMAS, that is, the thicker ice extends further into the  
 374 marginal ice zone. PIOMAS has a lower ice extent than the observations (Figure 3), al-



351 **Figure 3.** Sea ice thickness (m) in September 2012 for (a) CMST and (b) PIOMAS. Note  
 352 that the black contoured line indicates sea ice concentration of 15% retrieved from AMSR-E  
 353 using the Bootstrap algorithm by University of Bremen.

375 though sea ice concentration data are also used to constrain the model. There are no in-  
 376 dependent thickness observations to decide which of these two thickness fields are more  
 377 realistic, but the similar differences between ICESat and PIOMAS from October to Novem-  
 378 ber in the period 2003 to 2007 (Schweiger et al., 2011, their Figure 6) suggest that there  
 379 is not enough ice in the PIOMAS solution. It is plausible that the thicker ice in March  
 380 in CMST (Figure 1a), which is mainly due to the assimilation of CryoSat-2 data, pre-  
 381 conditions the system to lead to thicker and hence more realistic ice in September.

## 382 4.2 Comparison with In-situ Observations

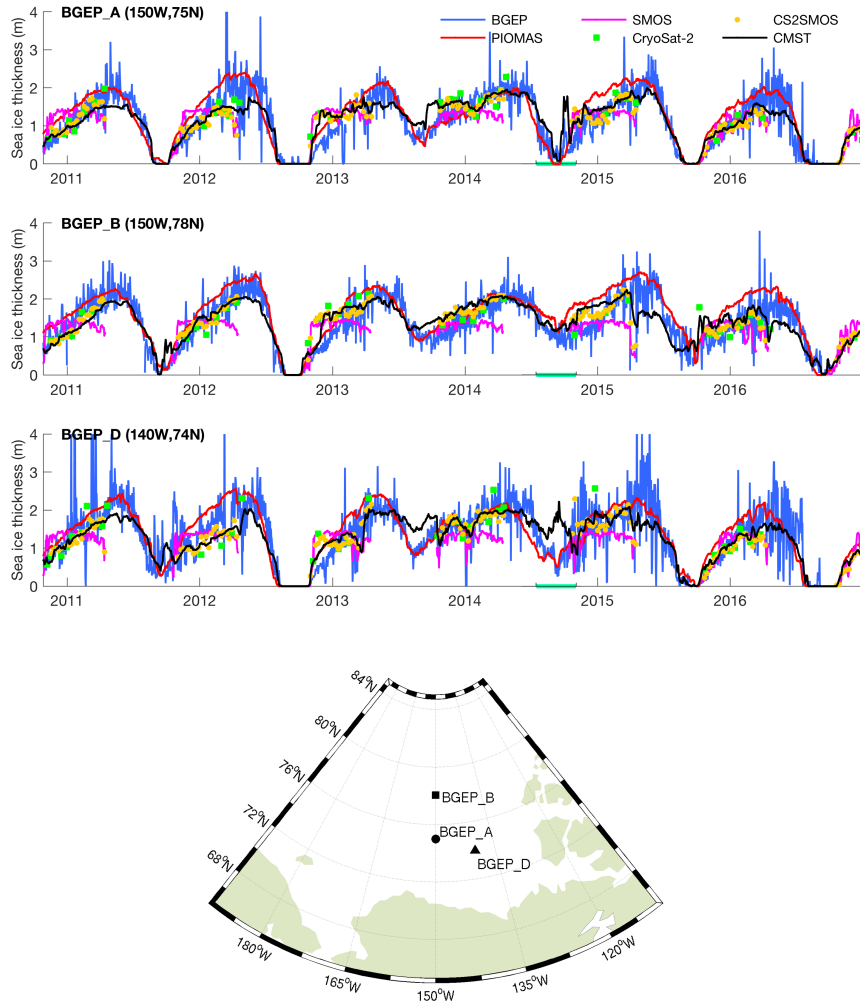
### 383 4.2.1 Comparison to BGEP ULS Data

384 The annual cycle and the inter-annual variability of ice thickness are reproduced  
 385 both in CMST and PIOMAS at all three mooring locations BGEP\_A, BGEP\_B and BGEP\_D  
 386 (Figure 4). As PIOMAS, the CMST estimate also reproduces the rapid decline of ice thick-  
 387 ness during melt seasons, when no satellite thickness data are available. All data that  
 388 went into CS2SMOS are also assimilated into CMST, so it is not surprising that CMST  
 389 is closer to CS2SMOS than PIOMAS. When the satellite data do not agree with the in-  
 390 situ ULS-data (e.g., in winter of 2012/2013 at BGEP\_A, BGEP\_B, and BGEP\_D or in  
 391 winter of 2013/2014 at BGEP\_A), the CMST does neither and the PIOMAS thickness

392 is closer to the in-situ data. At other times (e.g., most of the record in the freezing sea-  
393 son) the satellite thickness corrects CMST and leads to a better fit to the in-situ data  
394 than those of PIOMAS thickness estimates. PIOMAS tends to have a positive bias re-  
395 lative to satellite thickness during ice growing periods. This is consistent with the find-  
396 ing that the initial growth rates in numerical models are generally too large compared  
397 to observations possibly because they are too sensitive to the demarcation thickness pa-  
398 rameter  $H_0$  (Johnson et al., 2012). The assimilation of ice thickness reduces the lower  
399 ice growth rate in CMST estimates. However, the satellite thickness assimilated in late  
400 April (e.g., in 2015 and 2016 at BGEP\_B) also introduces biases, which leads the model  
401 to be not able to reach its local annual thickness maximum.

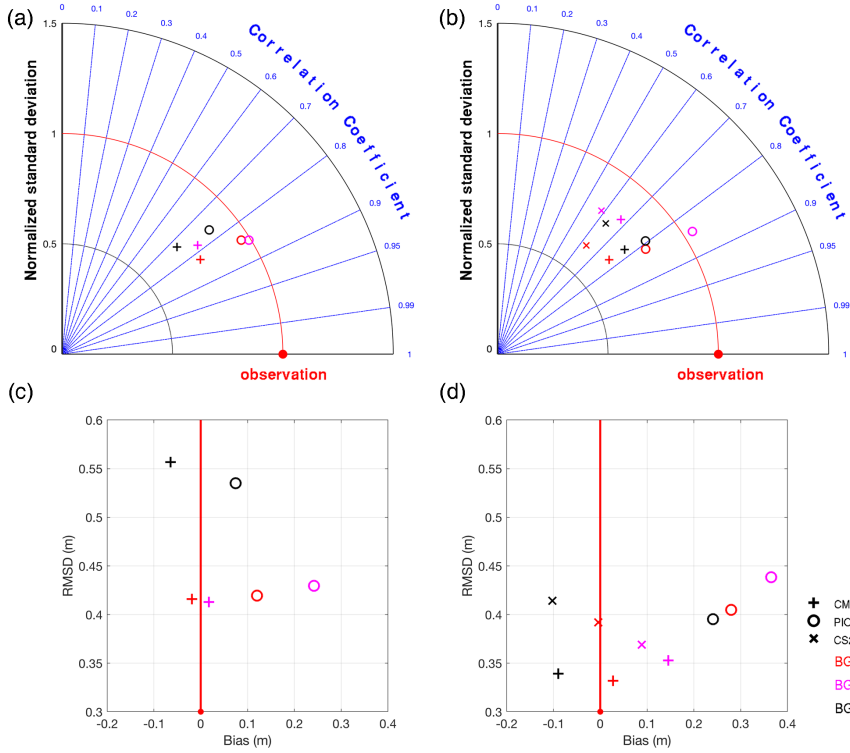
414 CMST captures the high fluctuation of sea ice thickness at BGEP\_A in 2014 (specif-  
415 ically the period marked in green in Figure 4) although with higher values compared to  
416 observations, while at BGEP\_D, CMST reproduces too thick ice. This different behav-  
417 ior is because sea ice concentration and thickness are not correlated very well in nature  
418 over the melting hiatus periods. The assimilation will occasionally generate abnormal  
419 values of thickness in the marginal ice zones due to abrupt ice concentration increase trig-  
420 gered by wind convergence. In the absence of thickness data, ice thickness is still cor-  
421 rected by ice concentration data by means of the error-covariance between thickness and  
422 concentration. This covariance is approximated in LESTKF so that the CMST thick-  
423 ness during summer cannot be as reliable as in winter and biases can also develop. When  
424 thickness data become available again, these biases are quickly corrected. This is very  
425 obvious in the thickness time series in October, 2013 at BGEP\_D. In 2014, ensemble forc-  
426 ing was not available from June to October. Interestingly, large summer biases develop  
427 that are probably caused by the suboptimal “ersatz” procedure of applying a forgetting  
428 factor (Yang et al., 2015a).

429 The fit of CMST, PIOMAS, and CS2SMOS to the BGEP ULS-data is summarized  
430 in Figure 5. At all three locations (BGEP\_A, BGEP\_B, BGEP\_D), PIOMAS thickness  
431 correlates slightly better with the in-situ observations than CMST and CS2SMOS (Fig-  
432 ures 5a and 5b). CMST correlates better with observations than CS2SMOS (Figure 5b).  
433 No product can reproduce the daily variability of the observed thickness shown in Fig-  
434 ure 4, but the standard deviations of the PIOMAS estimates are closer to the observa-  
435 tions (1.0 m) at all three locations.



402 **Figure 4.** Time series of sea ice thickness (m) for BGEP ULS data (blue), SMOS (magenta),  
 403 CS2SMOS (orange dot), PIOMAS (red), CryoSat-2 (green square), and CMST (black) at BGEP  
 404 moorings BGEP\_A, BGEP\_B and BGEP\_D. The short period without ensemble forcing for  
 405 CMST is marked in green on the time axis. Locations of ULS moorings BGEP\_A (75°N, 150°W),  
 406 BGEP\_B (78°N, 150°W) and BGEP\_D (74°N, 140°W) are represented by dot (●), square (■)  
 407 and triangle (▲), respectively.





408 **Figure 5.** Normalized Taylor diagram (a, b) and RMSD versus bias (c, d) for CMST (+),  
 409 PIOMAS (o) and CS2SMOS (x) with respect to BGEF observations at BGEF\_A (red), BGEF\_B  
 410 (magenta) and BGEF\_D (black). (a, c) are computed over the period when BGEF ULS-data  
 411 are available and (b, d) are computed for the CS2SMOS period (i.e. without melting season).  
 412 In Taylor diagrams the normalized standard deviation is on the radial axis and the correlation  
 413 coefficient is on the angular axis. The observations are indicated by red dots.

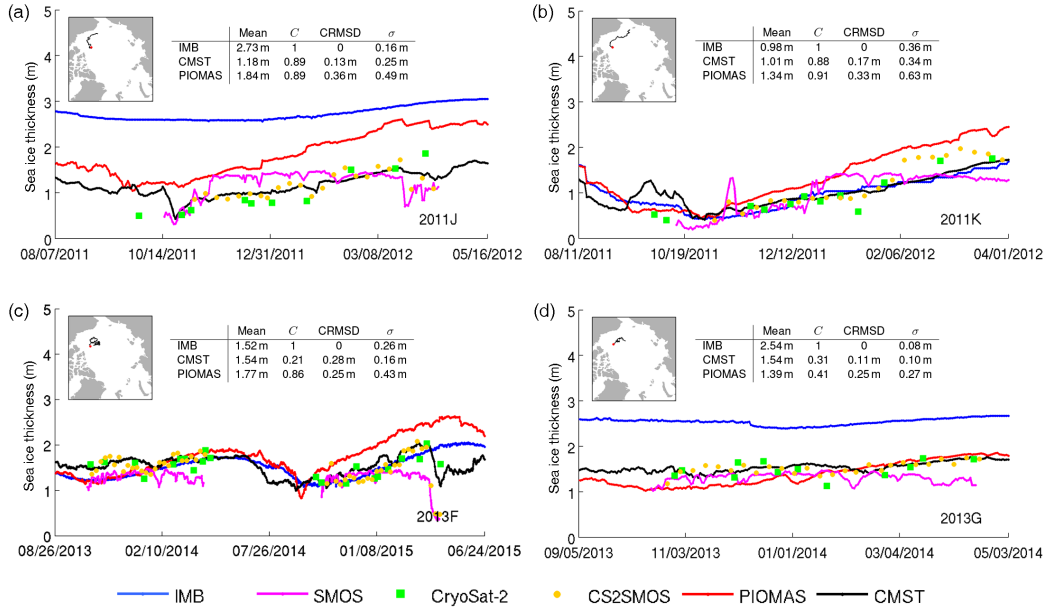
436 The CMST biases relative to the ULS-data are smaller than for PIOMAS (Figures 5c  
 437 and 5d). The positive biases of PIOMAS suggest that PIOMAS overestimates the thick-  
 438 ness especially in the freezing season. The RMSD of PIOMAS thickness is a little smaller  
 439 than for CMST at BGEF\_D, when the summer season is included (Figure 5c), but much  
 440 larger at BGEF\_B (Figures 5c, 5d, and 4b). The biases of CMST and CS2SMOS are sim-  
 441 ilar, but note that here CMST has a lower RMSD than CS2SMOS. Comparison between  
 442 Figures 5c and 5d also suggests that larger deviations with respect to observations for  
 443 CMST are mostly in the melting season, which can also be found directly in Figure 4.

#### 444 **4.2.2 Comparison to IMB Buoy Data**

445 Lagrangian buoy data are very useful for studying local growth and melt processes  
 446 together with 1-D column models of ice thermodynamics (e.g., Cheng et al., 2014). It  
 447 is less straightforward to compare the grid averaged results of an Eulerian ice-ocean model  
 448 to Lagrangian point observations. This is particularly true for sea ice thickness that is  
 449 always subject to large scale dynamic deformation processes and/or local ridging. That  
 450 the complex mixture of leads, first-year ice and multi-year ice often occur over distances  
 451 of only tens of meters makes the situation even worse (Perovich & Richtermenge, 2006).  
 452 Therefore we do not expect a very good agreement between gridded sea ice thickness vari-  
 453 ability and IMB buoys data along each trajectory.

454 Still, IMB buoy data provide information about temporal and spatial variability  
 455 of sea ice thickness that can be used to evaluate model results given the appropriate met-  
 456 ric. For our comparisons, we selected 32 IMB buoys with sufficiently long observation  
 457 records during the period from October 2010 to December 2016. To improve the agree-  
 458 ment between IMB buoy data and gridded products, the thickness biases can be adjusted  
 459 in the buoy data to focus on the subsequent thickness evolutions (Lei et al., 2014). The  
 460 underlying assumption is that the ice surface and oceanic heat flux are the same for the  
 461 IMB buoy data and the gridded (model) data. This assumption works best when ther-  
 462 modynamic processes dominate and snow does not confound the heat balance. During  
 463 initial inspection, we also found systematic differences between IMB buoy data, CMST  
 464 and PIOMAS along the buoy trajectories. Figure 6 shows four selected cases that illus-  
 465 trate the systematic biases. These differences can be reduced by removing the mean thick-  
 466 ness of each data set (not shown, but Figures 6a and 6d are obvious examples). There-  
 467 fore, we compute the CRMSD, which removes the mean of time series, and the standard  
 468 deviations of the time series, which measure the variability of sea ice thickness, as eval-  
 469 uation metrics. The metrics are summarized in Taylor diagrams (Figure 7).

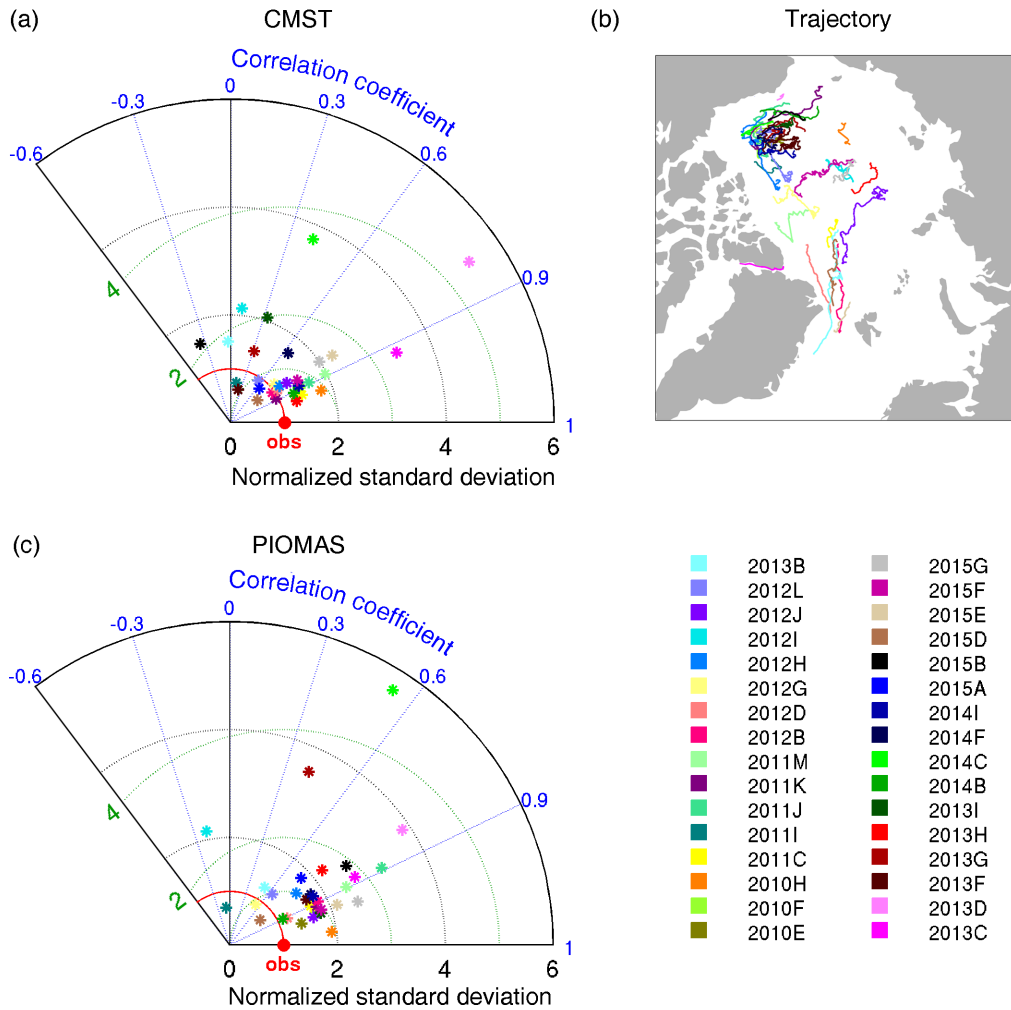
475 In general, CMST standard deviations are closer to observations than PIOMAS stan-  
 476 dard deviations; the CRMSDs are also smaller for CMST, but PIOMAS correlates bet-  
 477 ter with IMB buoy data (Figures 7a and 7c). The mean normalized standard deviation  
 478 of CMST is 1.63, while that of PIOMAS is 2.00; the mean normalized CRMSD for CMST  
 479 is 3.37 and that for PIOMAS is 3.63. The correlations for CMST and PIOMAS are 0.66  
 480 and 0.76, respectively. Some of these statistical differences between CMST and PIOMAS



470 **Figure 6.** Sea ice thickness (m) time series: IMB buoy data (blue), SMOS (magenta),  
 471 CryoSat-2 (green squares), CS2SMOS (orange dots), CMST (black), and PIOMAS (red) on  
 472 each IMB buoys trajectory shown in the top left corner. The deployment location of the IMB is  
 473 indicated by a red dot on the trajectory. The statistics for IMB buoy data, CMST, and PIOMAS  
 474 are also shown in each plot. The date format is mm/dd/yyyy.

481 are expected, because the sea ice thickness assimilation adds information that should im-  
 482 prove realism of the model on average, but at the same time can also introduce abrupt  
 483 jumps when new data become available. Assimilating data that are not consistent with  
 484 the model can hence lead to lower correlations. The better standard deviations of CMST  
 485 suggest that CMST reproduces the thickness variability of IMB buoy data better than  
 486 PIOMAS on longer time scales.

491 We now discuss four representative time series (Figure 6). Along the trajectories  
 492 of buoys 2011J (Figure 6a, 8 months, August 2011 to May 2012) and 2013G (Figure 6d,  
 493 7 months, September 2013 to May 2014), CMST is mostly constrained by CryoSat-2 thick-  
 494 ness data and hence close to CS2SMOS, but the IMB buoy data, as in many other cases  
 495 not shown, implies much thicker ice. In these cases, we assume that the IMB buoy lo-  
 496 cation on the floe does not necessarily represent a large spatial average and the mean  
 497 cannot be compared to the gridded model data. Instead the buoy provides useful infor-  
 498 mation on sea ice thickness evolution. The CRMSD of CMST with respect to 2011J is



487 **Figure 7.** Taylor diagrams of (a) CMST and (c) PIOMAS with respect to all available IMB  
 488 buoy data from October 2010 to December 2016. The green dotted lines indicate the normalized  
 489 CRMSD. The trajectories of all the IMB buoys are shown in (b). The reference observations are  
 490 indicated by “obs” in red.

499 0.13 m, while that of PIOMAS is 0.36 m. The PIOMAS thickness is larger than the es-  
 500 timates by CMST and satellite data and overestimates the trend in the buoy data. At  
 501 buoy 2013G, CMST, PIOMAS and CS2SMOS are very similar. Still, the CRMSD of CMST  
 502 with respect to 2013G is 0.11 m and that of PIOMAS is 0.25 m implying a slightly bet-  
 503 ter thickness variability in CMST.

504 In some cases, the data assimilation rejects satellite thickness data that are incon-  
 505 sistent with the model dynamics. At buoy 2011K (Figure 6b, 7 months, August 2011 to  
 506 April 2012), this happens between February 1st 2012 and April 1st 2012, when CrySat-

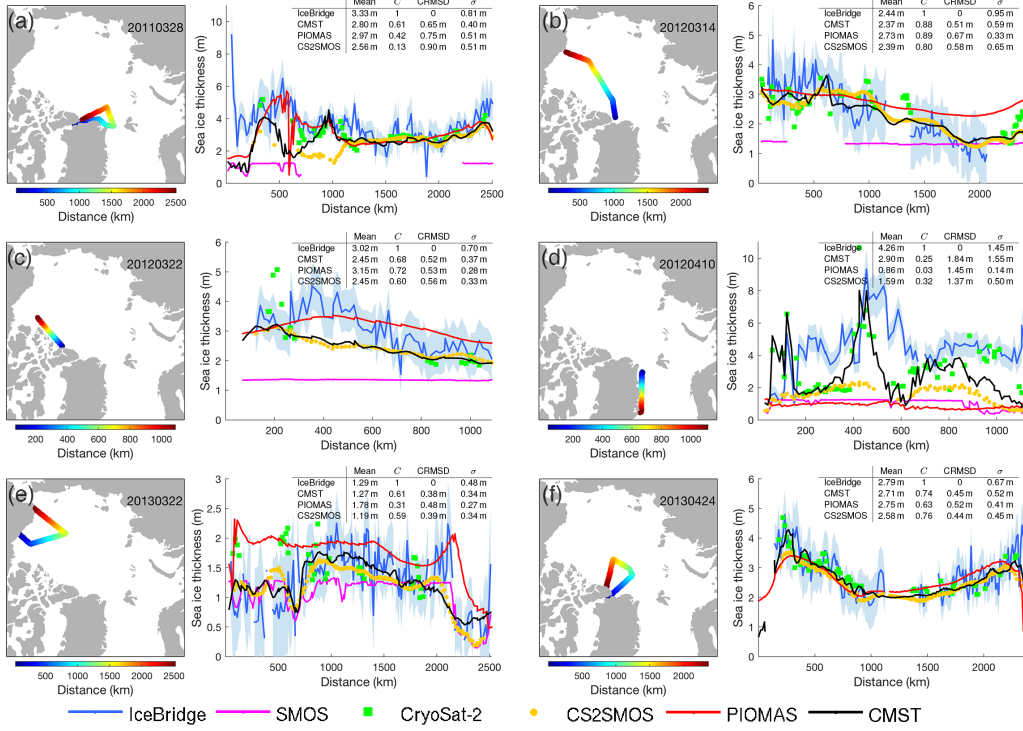
2 thickness data tends to be too large. As a consequence, the CMST thickness, some-  
 508 what fortuitously, agrees better with the IMB buoy data than CS2SMOS and PIOMAS,  
 509 both of which also overestimate the thickness. In contrast, ice thickness in CMST is first  
 510 too low and then becomes too large in September 2011, which we attribute to the as-  
 511 simulation of ice concentration with inaccurate covariances between thickness and con-  
 512 centration. Buoy 2013F (Figure 6c, 22 months, August 2013 to June 2015) recorded thick-  
 513 ness for nearly two years. Both CMST and PIOMAS show plausible seasonal thickness  
 514 variability, but PIOMAS tends to overestimate thickness after the summer of 2014 and  
 515 the CMST thickness drops sharply in spring 2015 probably due to the impact of assim-  
 516 ilating SMOS thickness data which also drops very quickly. The CRMSDs of CMST and  
 517 PIOMAS are similar with values of 0.27 m and 0.24 m.

518 Another example of a strong jump in thickness in CMST can be found in 2011J  
 519 in mid-October (Figure 6a). Here, the jump is associated with the availability of thick-  
 520 ness data. During summer, the model without thickness assimilation (because there are  
 521 no data available in summer) develops a bias and is inconsistent with the thickness data  
 522 in October. Data assimilation quickly corrects this bias leading to the observed jump  
 523 in the time series. This phenomenon can only be avoided by a data assimilation scheme  
 524 that also takes into account future observations, for example a Kalman smoother (Evensen  
 525 & Van Leeuwen, 2000), or full 4D-VAR state estimation as in ECCO (Forget et al., 2015).

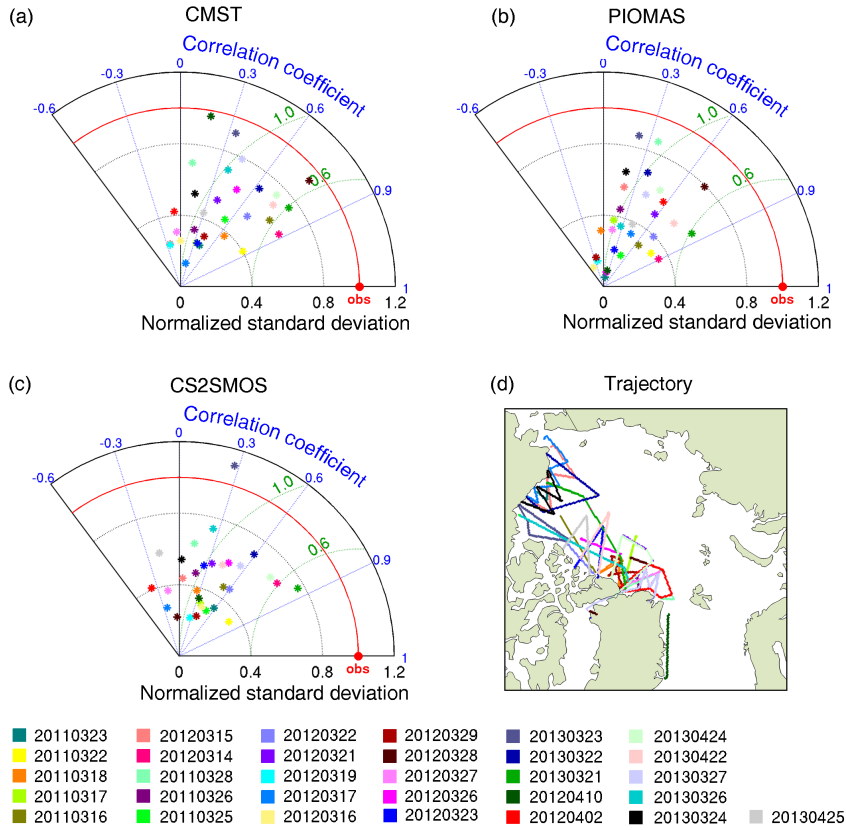
### 526 ***4.2.3 Comparison to Operation IceBridge Data***

527 The Operation IceBridge campaigns that are always conducted in March and April  
 528 allow a meaningful comparison also to CS2SMOS. 31 airborne campaigns in 2011, 2012,  
 529 and 2013 are selected for the comparison. Individual campaigns are short (order of hours),  
 530 so that the variability along flight tracks represents spatial, but not temporal variabil-  
 531 ity. In order to gain insight into spatial variations of different thickness products, the  
 532 sections (e.g., Figure 8) are defined along the IceBridge trajectories without further tak-  
 533 ing into account the real flight routes in this study.

547 The general performance of the CMST, PIOMAS, CS2SMOS thickness datasets  
 548 with respect to IceBridge thickness is summarized in Taylor plots (Figure 9). Accord-  
 549 ing to these metrics no dataset stands out clearly. CMST has the best average normal-  
 550 ized standard deviation with 0.52 compared to PIOMAS (0.41) and CS2SMOS (0.48),



534 **Figure 8.** Sea ice thickness along Operation IceBridge trajectories. The trajectory of each  
 535 campaign is shown on the map to the left of each plot, and colors indicate the distance from the  
 536 starting point. The sea ice thickness of IceBridge (blue), SMOS (magenta), CryoSat-2 (green  
 537 square), CS2SMOS (orange dot), PIOMAS (red) and CMST (black) in the right hand side plots  
 538 are plotted against track distance. The shaded areas represent the uncertainties of IceBridge  
 539 thickness as provided in the dataset. The statistics of IceBridge, PIOMAS, CMST and CS2SMOS  
 540 sea ice thickness along the trajectories are also shown in each plot. Note that these statistics are  
 541 computed over the overlapping periods of the four datasets.



542 **Figure 9.** Taylor diagrams of (a) CMST, (b) PIOMAS and (c) CS2SMOS with respect to  
 543 all IceBridge operations available in 2011, 2012 and 2013. The trajectories of all operations are  
 544 shown in (d). The green dotted lines indicate the normalized CRMSD. The reference observa-  
 545 tions are represented by “obs” in red. Note that the Taylor diagram of CS2SMOS is calculated  
 546 over area where CS2SMOS thickness is available.

551 but in all datasets the variability is smaller than in the observations. The mean normal-  
552 ized CRMSDs of 1.13 (CMST), 1.12 (PIOMAS), and 1.17 (CS2SMOA) are very simi-  
553 lar, with CMST and PIOMAS outperforming CS2SMOS slightly. In contrast to com-  
554 parisons with BGEP ULS and IMB buoy data, where PIOMAS correlated best with ob-  
555 servations, the CMST estimates have the best mean correlation of 0.40 with IceBridge  
556 measurements; the correlation coefficient is 0.35 for PIOMAS and 0.32 for CS2SMOS.  
557 In summary, the CMST agrees slightly better with the IceBridge thickness data than PI-  
558 OMAS and CS2SMOS.

559 We discuss six (one in 2011, three in 2012, and two in 2013) representative exam-  
560 ples of the 31 selected IceBridge campaigns in greater detail (Figure 8). Some of these  
561 selected sections (20110328, 20120314 and 20130424, Figures 8a, 8b and 8f) are repeat  
562 sections and others are focused on specific areas (20120322, 20120410 and 20130322, Fig-  
563 ures 8c, 8d and 8e). Together, the selected sections illustrate all aspects of the perfor-  
564 mances of the different products.

565 Section 20130424 (Figure 8f) and the first 1000 km of 20120314 (Figure 8b) serve  
566 as examples of good agreement of CMST, PIOMAS, and CS2SMOS with IceBridge thick-  
567 ness estimates with maximum deviations of 0.25 m. Based on satellite data, CMST and  
568 CS2SMOS reproduce the transition from multi-year ice to first-year ice accurately along  
569 section 20120314 (Figure 8b). The same is true for the repeated section 20130321 one  
570 year later (not shown). In contrast, PIOMAS tends to overestimate the sea ice thick-  
571 ness in the thin ice area north of Alaska. In the following year, a similar PIOMAS bias  
572 is also found for section 20130322 in the Beaufort Sea (Figure 8e) (see also Schweiger et  
573 al., 2011; Johnson et al., 2012; Wang et al., 2016).

574 Some of the extreme thicknesses in the Nares Strait (Figure 8a), the Lincoln Sea  
575 (Figure 8f), and north of the CAA (Figure 8c) are not accurately represented in neither  
576 CMST, PIOMAS, or CS2SMOS. In these multi-year ice regions, the ice is heavily de-  
577 formed and ridged, so that satellite observations are difficult: thin ice  $< 1$  m, formed in  
578 leads opened by strong wind events, can be observed with SMOS and heavily ridged, thick  
579 multi-year ice with CryoSat-2 (Haas et al., 2006), so that conflicting thickness estimates  
580 in close proximity are possible. In combination, these data can lead to lower thicknesses  
581 as in CS2SMOS, or to some extent in CMST. In the Nares Strait (beginning of section  
582 20110328 in Figure 8a), CMST clearly follows the SMOS thickness data, which is thin-



583 ner by 3 m and more than the IceBridge estimate, because there is no CryoSat-2 data  
584 available to measure thick ice. Further, the resolution of the model (18 km) is not suf-  
585 ficient to resolve narrow straits accurately (we use 2 to 3 grid points across the Nares  
586 Strait), so that the model likely has a bias in this area anyway.

587 Guided by CryoSat-2 data, the thickness along the east coast of Greenland is best  
588 represented in CMST (Figure 8d). Both PIOMAS and CS2SMOS (probably due to the  
589 influence of SMOS data) strongly underestimate the thickness in this dynamical outflow  
590 region. The CMST is also too thin most of the time, but captures some of the variabil-  
591 ity and extreme thicknesses along the track. The PIOMAS thickness (like the SMOS thick-  
592 ness) is flat along this section and very thin.

## 593 **5 Discussions**

594 As shown above, our model ice thickness estimates show some advantages over PI-  
595 OMAS and fill the summer gaps of CS2SMOS. At the BGEP mooring, our CMST es-  
596 timates agree better with CS2SMOS than the PIOMAS thickness, because the same thick-  
597 ness data was used in both estimates. Both ULS-data derived thickness and satellite de-  
598 rived thickness contain errors, but the satellite thickness assimilation further improves  
599 the model mean estimates at the cost of reduced variability and correlations. The bet-  
600 ter standard deviations and CRMSDs with respect to the IMB trajectories indicate that  
601 the CMST thickness agrees better with IMB data than the other datasets. All datasets  
602 can reproduce many aspects of the IceBridge thickness tracks, but none of the datasets  
603 represents ridged ice accurately. PIOMAS tends to overestimate the thickness in thin  
604 ice regions and appears to underestimate the spatial variability. The added value of thick-  
605 ness assimilation gives CMST an advantage over the model solution PIOMAS. In some  
606 places, where CS2SMOS does not compare well with IceBridge data because of conflicts  
607 between SMOS and CryoSat-2 data, the additional physics of the numerical model in  
608 CMST appears to reconcile these conflicts. These difference between SMOS and CryoSat-  
609 2 data can be also found in Baffin Bay and in regions where ice drifts fast (Mu et al.,  
610 2018). The purely statistical method CS2SMOS cannot reconcile these differences be-  
611 cause it has only available statistical prior knowledge (data uncertainties). Regardless  
612 of the temporal and spatial coverage of the satellite trajectories, CMST provides daily  
613 mean thickness on model grids. CS2SMOS data, however, are rather weekly snapshots.

614 The model we used is forced by atmospheric ensemble forcing by which the uncer-  
615 tainties of air-sea or air-ice flux exchanges are explicitly estimated by the ocean ensem-  
616 ble. During the data assimilation, the ensemble spread will persist without the require-  
617 ment of further applying the artificial inflation. Uncertainties of the CMST estimates  
618 can also be generated from the ensemble spread as a by-product.

619 The main limitation of the CMST estimates is that it relies heavily on the qual-  
620 ity of satellite data products and the parameterizations of physical processes in the model.  
621 The retrieval of CryoSat-2 thickness is based on the hydrostatic equilibrium assumption.  
622 Whether this is still appropriate in the ridged ice area along northern coast of CAA or  
623 in the fast ice area such as the Siberian Seas is still not clear. The validation of the snow  
624 thickness climatology used for CryoSat-2 thickness retrieval in recent years also needs  
625 further investigation. Satellite thickness data conflicts would lead to larger uncertain-  
626 ties in our final product. Examples of these conflicts can be found along the northern  
627 coast of Greenland where open water forms, east of Greenland where there are ice floes  
628 and in the Baffin Bay where snow climatology is not applicable for thickness retrieval.

629 In addition, the assimilation of sea ice concentration in the early freezing period  
630 in late summer will occasionally lead to unrealistically thick ice in marginal ice zones in  
631 the CMST estimates. This cannot be circumvented in the current implementation. A  
632 possible remedy may be applying a threshold to the thickness correction, but exploring  
633 the details of such an algorithm requires a dedicated investigation beyond the scope of  
634 our work.

635 In the Siberian Seas, the satellite thickness assimilation improves the ice thickness  
636 estimates of CMST over those of PIOMAS. Simulating the Siberian Seas with sea ice  
637 models without data assimilation requires the parameterization of land fast ice processes  
638 or modifications on ice ridging dynamics. In an evaluation of ice thickness by six mod-  
639 els including the MITgcm in a very similar configuration, the models generally tend to  
640 overestimate the thickness in the regions of flat immobile landfast ice especially in the  
641 Siberian Seas (Johnson et al., 2012). These systematic errors are expected to persist be-  
642 cause landfast ice is neither parameterized nor resolved in the model(s) (Lemieux et al.,  
643 2016). The CMST estimate appears to reject the satellite thickness in the Siberian Seas  
644 because of the large data uncertainties, but the model dynamics produce too thick sea  
645 ice. This bias may be alleviated by tuning or improving the ice strength and ridging pa-

parameterization. In our setup, ridging is parameterized by restricting sea ice fractional area to values  $\leq 1$  (Schulkes, 1995). Model parameters such as albedo, compressive strength, demarcation thickness  $H_0$  for lead closing, etc. will also play a big part in simulating thickness variations and spatial distributions, particularly when satellite thickness is unavailable in melt seasons. These parameters are currently not well constrained. Therefore, uncertainties of the CMST estimates also result from potentially incomplete parameterizations of physical processes in the model. The effects of parameter choices are ignored in this study.

The comparison of model and data products also provides some insight into the uncertainties in different ice thickness measurements. The deviations between the satellite thickness and ULS in late April (Figure 4) imply that more cross validations are necessary to improve thickness retrievals. Comparing IMBs (or Lagrangian data in general) to large-scale models is delicate and requires a careful evaluation of the data on Eulerian grids. Still, a distributed network of IMBs may provide an opportunity to assess the performances of different data products. The near-future Multidisciplinary drifting Observatory for the Study of Arctic Climate (MOSAiC; <http://www.mosaicobservatory.org/>) is expected to conduct such observations. Uncertainties of IceBridge thickness stem from uncertainties in snow detection and spatially and temporally varying ice and snow densities (Kurtz et al., 2013). The IceBridge footprint is only 40 m. In this way thickness data statistics are biased in the along track direction and cannot take into account the cross track variability. In contrast, the smallest model element is a grid cell with cell width  $\sim 18$  km.

## 6 Conclusions

Daily entire Arctic sea ice thickness estimates are obtained from combining remotely sensed sea thickness and concentration data with a sea ice-ocean model. These thickness estimates are available at all times for the entire CryoSat-2 period 2010–2016 closing the satellite thickness observation gap in summer with the help of model dynamics and concentration data assimilation. The additional thickness data in combination with a sophisticated data assimilation scheme helps to reduce biases that are still present in current sea ice thickness products. The generated CMST estimates that take advantage of satellite thickness observations and physics of the sea ice-ocean model can be viewed

677 as an optimal compromise between CS2SMOS and PIOMAS insofar as it combines the  
678 strengths of both products (thickness observations and model dynamics).

679 Our main findings are that the CMST is relatively close to the CS2SMOS data, which  
680 is not surprising as both use the same thickness data. The thickness data help to reduce  
681 some biases present in other models, but in general the comparison with in-situ thick-  
682 ness data turns out to be similar to that of PIOMAS thickness to in-situ data. Because  
683 we use a model, the thickness estimates can be extended into the summer season, where  
684 adequate initial conditions together with appropriate surface forcing help to simulate re-  
685 alistic summer sea ice thicknesses.

686 The new Arctic sea ice thickness estimate CMST provides an opportunity to study  
687 the ice volume changes in recent years. The difference maps between CMST and PIOMAS  
688 suggest areas where more in-situ sea ice thickness measurements would help reconcile  
689 the models with data. Moreover, we expect that this dataset will serve as a good refer-  
690 ence for parameterizations for sea ice models.

## 691 **Acknowledgments**

692 We thank Ruibo Lei from the Polar Research Institute of China for the discussions about  
693 the data processing of the IMB buoys, Jinlun Zhang from the University of Washington  
694 for providing the PIOMAS sea ice thickness data and comments on the manuscript, and  
695 Xi Liang from National Marine Environmental Forecasting Center for the suggestions  
696 on sea ice assimilation. We thank the University of Hamburg for providing SMOS sea  
697 ice thickness data and the ASI-SSMI sea ice concentration data, National Snow and Ice  
698 Data Center (NSIDC) for providing the IceBridge thickness data, the Woods Hole Oceanog-  
699 raphic Institution for the sea ice draft data, the Cold Regions Research and Engineer-  
700 ing Laboratory for IMB data, and the European Centre for Medium-Range Weather Fore-  
701 casts for the UKMO ensemble forecasting data. This study is supported by the National  
702 Natural Science Foundation of China (41706224, 41776192), the National Key R&D Pro-  
703 gram of China (2018YFA0605901), the BMBF (Federal Ministry of Education and Re-  
704 search, Germany)-SOA (State Oceanic Administration, China) Joint Project (01DO14002),  
705 the Federal Ministry of Education and Research of Germany in the framework of SSIP  
706 (grant01LN1701A) and the Key Research Program of Frontier Sciences of Chinese Academy  
707 of Sciences (grant No. QYZDY-SSW-DQC021). Contribution by SNL is partly made in  
708 the framework of the state assignment of FASO Russia (theme No. 0149-2018-0014) and

709 the BMBF ERA-Net project EXOSYSTEM (grant 01DJ16016). The CMST data in this  
 710 paper are archived in PANGAEA and available at [https://doi.pangaea.de/10.1594/](https://doi.pangaea.de/10.1594/PANGAEA.891475)  
 711 [PANGAEA.891475](https://doi.pangaea.de/10.1594/PANGAEA.891475).

## 712 References

- 713 Blockley, E. W., & Peterson, K. A. (2018). Improving met office seasonal forecasts  
 714 of arctic sea ice using assimilation of cryosat-2 thickness. *The Cryosphere Discus-*  
 715 *sions*, 2018, 1–31. doi: 10.5194/tc-2018-62
- 716 Bowler, N. E., Arribas, A., Mylne, K. R., Robertson, K. B., & Beare, S. E. (2008).  
 717 The MOGREPS short-range ensemble prediction system. *Quart. J. Roy. Meteor.*  
 718 *Soc.*, 134(632), 703–722. doi: 10.1002/qj.234
- 719 Brodzik, M. J., Billingsley, B., Haran, T., Raup, B., & Savoie, M. H. (2012). EASE-  
 720 Grid 2.0: Incremental but significant improvements for earth-gridded data sets.  
 721 *ISPRS Int. J. Geo-Information*, 1(3), 32–45. doi: 10.3390/ijgi1010032
- 722 Cheng, B., Vihma, T., Rontu, L., Kontu, A., Duguay, H. K. P. C., & Pulliainen, J.  
 723 (2014). Evolution of snow and ice temperature, thickness and energy balance in  
 724 Lake Orajärvi, northern Finland. *Tellus A*, 66(1).
- 725 Day, J. J., Hawkins, E., & Tietsche, S. (2014). Will Arctic sea ice thickness initial-  
 726 ization improve seasonal forecast skill? *Geophys. Res. Lett.*, 41, 7566–7575. doi:  
 727 10.1002/2014GL061694
- 728 Evensen, G., & Van Leeuwen, P. J. (2000). An ensemble kalman smoother for non-  
 729 linear dynamics. *Monthly Weather Review*, 128(6), 1852–1867.
- 730 Flato, G., Marotzke, J., Abiodun, B., Braconnot, P., Chou, S., Collins, W., . . . For-  
 731 est, C. (2013). *Climate change 2013: The Physical Science Basis. Contribution of*  
 732 *Working Group I to the Fifth Assessment Report of the Intergovernmental Panel*  
 733 *on Climate Change, chap. Evaluation of Climate Models*, 126 pp. Cambridge  
 734 University Press, Cambridge, United Kingdom and New York, NY, USA.
- 735 Forget, G., Campin, J., Heimbach, P., Hill, C., Ponte, R., & Wunsch, C. (2015).  
 736 Ecco version 4: An integrated framework for non-linear inverse modeling and  
 737 global ocean state estimation. *Geoscientific Model Development*, 8(10), 3071–  
 738 3104. doi: 10.5194/gmd-8-3071-2015
- 739 Francis, J. A., Chan, W., Leathers, D. J., Miller, J. R., & Veron, D. E. (2009).  
 740 Winter Northern Hemisphere weather patterns remember summer Arctic sea-ice

- 741 extent. *Geophys. Res. Lett.*, *36*(7). doi: 10.1029/2009GL037274
- 742 Gaspari, G., & Cohn, S. E. (1999). Construction of correlation functions in two and  
743 three dimensions. *Quart. J. Roy. Meteor. Soc.*, *125*, 723–757.
- 744 Haas, C., Hendricks, S., & Doble, M. (2006). Comparison of the sea-ice thickness  
745 distribution in the lincoln sea and adjacent arctic ocean in 2004 and 2005. *Annals  
746 of glaciology*, *44*, 247–252.
- 747 Haine, T. W., Curry, B., Gerdes, R., Hansen, E., Karcher, M., Lee, C., . . .  
748 Woodgate, R. (2015). Arctic freshwater export: Status, mechanisms, and  
749 prospects. *Global and Planetary Change*, *125*, 13–35.
- 750 Hess, S. L. (1959). *Introduction to theoretical meteorology*. New York, NY: Holt,  
751 Rinehart, and Winston.
- 752 Hibler III, W. (1979). A dynamic thermodynamic sea ice model. *Journal of Physical  
753 Oceanography*, *9*(4), 815–846.
- 754 Janjić, T., Bormann, N., Bocquet, M., Carton, J., Cohn, S., Dance, S., . . . Weston,  
755 P. (2017). On the representation error in data assimilation. *Quarterly Journal of  
756 the Royal Meteorological Society*.
- 757 Johnson, M., Proshutinsky, A., Aksenov, Y., Lindsay, A. T. N. R., Haas, C., Zhang,  
758 J., . . . de Cuevas, B. (2012). Evaluation of Arctic sea ice thickness simulated  
759 by Arctic Ocean Model Intercomparison Project models. *J. Geophys. Res.*,  
760 *117*(C00D13). doi: 10.1029/2011JC007257
- 761 Kaleschke, L., Lüpkes, C., Vihma, T., Haarpaintner, J., Bochert, A., Hartmann,  
762 J., & Heygster, G. (2001). SSM/I sea ice remote sensing for mesoscale ocean-  
763 atmosphere interaction analysis. *Can. J. Remote Sens.*, *27*(5), 526–537. doi:  
764 10.1080/07038992.2001.10854892
- 765 Kern, S., Kaleschke, L., & Spreen, G. (2010). Climatology of the nordic (Irminger,  
766 Greenland, Barents, Kara and White/Pechora) Seas ice cover based on 85 GHz  
767 satellite microwave radiometry: 1992-2008. *Tellus A*, *62*(4), 411–434. doi:  
768 10.1111/j.1600-0870.2010.00457.x
- 769 Kumar, A., Perlwitz, J., Eischeid, J., Quan, X., Xu, T., Zhang, T., . . . Wang, W.  
770 (2010). Contribution of sea ice loss to Arctic amplification. *Geophys. Res. Lett.*,  
771 *37*(21). doi: 10.1029/2010GL04502
- 772 Kurtz, N., Farrell, S., Studinger, M., Galin, N., Harbeck, J., Lindsay, R., . . . Son-  
773 ntag, J. (2013). Sea ice thickness, freeboard, and snow depth products from

- 774 operation icebridge airborne data. *The Cryosphere*, 7(4), 1035–1056. doi:  
775 10.5194/tc-7-1035-2013
- 776 Kurtz, N., Studinger, M., Harbeck, J., Onana, V., & Yi, D. (2015). Icebridge l4 sea  
777 ice freeboard, snow depth, and thickness, version 1. *NASA National Snow and Ice*  
778 *Data Center Distributed Active Archive Center, Boulder, Colorado, USA*. doi: 10  
779 .5067/G519SHCKWQV6
- 780 Kwok, R., Cunningham, G. F., Wensnahan, M., Rigor, I., Zwally, H. J., & Yi, D.  
781 (2009). Thinning and volume loss of the Arctic Ocean sea ice cover: 2003-2008. *J.*  
782 *Geophys. Res.*, 114(7). doi: 10.1029/2009JC005312
- 783 Laxon, S. W., Giles, K. A., Ridout, A. L., Wingham, D. J., Willatt, R., Cullen, R.,  
784 ... Davidson, M. (2013). Cryosat-2 estimates of Arctic sea ice thickness and  
785 volume. *J. Geophys. Res.*, 40(4), 732–737. doi: 10.1002/grl.50193
- 786 Lei, R., Li, N., Heil, P., Cheng, B., Zhang, Z., & Sun, B. (2014). Multiyear  
787 sea ice thermal regimes and oceanic heat flux derived from an ice mass bal-  
788 ance buoy in the Arctic Ocean. *J. Geophys. Res.*, 119(1), 537–547. doi:  
789 10.1002/2012JC008731
- 790 Lemieux, J.-F., Dupont, F., Blain, P., Roy, F., Smith, G. C., & Flato, G. M. (2016).  
791 Improving the simulation of landfast ice by combining tensile strength and a pa-  
792 rameterization for grounded ridges. *Journal of Geophysical Research: Oceans*,  
793 121(10), 7354–7368.
- 794 Lisæter, K. A., Evensen, G., & Laxon, S. W. (2007). Assimilating synthetic cryosat  
795 sea ice thickness in a coupled ice-ocean model. *J. Geophys. Res.*, 112(7), 1–14.  
796 doi: 10.1029/2006JC003786
- 797 Liu, J., Curry, J. A., Wang, H., Song, M., & Horton, R. M. (2012). Impact of declin-  
798 ing arctic sea ice on winter snowfall. *Proc. Nat. Acad. Sci. USA*, 109(11), 4074–  
799 4079. doi: 10.1073/pnas.1114910109
- 800 Losch, M., Menemenlis, D., Campin, J.-M., Heimbach, P., & Hill, C. (2010). On the  
801 formulation of sea-ice models. Part 1: Effects of different solver implementations  
802 and parameterizations. , 33(1–2), 129–144. doi: 10.1016/j.ocemod.2009.12.008
- 803 Marshall, J., Adcroft, A., Hill, C., Perelman, L., & Heisey, C. (1997). A finite-  
804 volume, incompressible Navier Stokes model for studies of the ocean on parallel  
805 computers. *J. Geophys. Res.*, 102(C3), 5753–5766. doi: 10.1029/96JC02775
- 806 Melling, H., Johnston, P., & Riedel, D. (1995). Measurements of the underside to-

- 807 pography of sea ice by moored subsea sonar. *J. Atmos. Oceanic Technol.*, *12*(3),  
808 589–602.
- 809 Menemenlis, D., Campin, J.-M., Heimbach, P., Hill, C., Lee, T., Nguyen, A., ...  
810 Zhang, H. (2008). ECCO2: High resolution global ocean and sea ice data synthe-  
811 sis. *Mercator Ocean Quarterly Newsletter*, *31*, 13–21.
- 812 Mu, L., Yang, Q., Losch, M., Losa, S. N., Ricker, R., Nerger, L., & Liang, X. (2018).  
813 Improving sea ice thickness estimates by assimilating cryosat-2 and smos sea ice  
814 thickness data simultaneously. *Quarterly Journal of the Royal Meteorological*  
815 *Society*, *144*(711), 529–538.
- 816 Mu, L., Zhao, J., & W., Z. (2017). Regime shift of the dominant factor for halo-  
817 cline depth in the Canada Basin during 1990-2008. *Acta Oceanol. Sin.*, *36*(1), 35–  
818 43. doi: 10.1007/s13131-016-0883-0
- 819 Nerger, L., & Hiller, W. (2013). Software for ensemble-based data assimilation sys-  
820 tems – implementation strategies and scalability. *Comput. Geosci.*, *55*, 110–118.  
821 doi: 10.1016/j.cageo.2012.03.026
- 822 Nerger, L., Janji, T., Schrter, J., & Hiller, W. (2012). A unification of ensemble  
823 square root kalman filters. *Monthly Weather Review*, *140*(7), 2335-2345.
- 824 Nguyen, A. T., Menemenlis, D., & Kwok, R. (2011). Arctic ice-ocean simulation  
825 with optimized model parameters: Approach and assessment. *J. Geophys. Res.*,  
826 *116*(C4). doi: 10.1029/2010JC006573
- 827 Overland, J. E., & Wang, M. (2010). Large-scale atmospheric circulation changes  
828 are associated with the recent loss of Arctic sea ice. *Tellus A*, *62*(1), 1–9. doi: 10  
829 .1111/j.1600-0870.2009.00421.x
- 830 Parkinson, C. L., & Washington, W. M. (1979). A large-scale numerical model of sea  
831 ice. *Journal of Geophysical Research: Oceans*, *84*(C1), 311–337.
- 832 Perovich, D., Richter-Menge, J., & Polashenski, C. (2009). *Observing and under-*  
833 *standing climate change: Monitoring the mass balance, motion, and thickness of*  
834 *arctic sea ice*. <http://imb-crrel-dartmouth.org>.
- 835 Perovich, D., & Richtermenge, J. A. (2006). From points to poles: extrapolat-  
836 ing point measurements of sea-ice mass balance. *Annals of Glaciology*, *44*(1),  
837 188-192.
- 838 Richter-Menge, J. A., Perovich, D. K., Elder, B. C., Claffey, K., Rigor, I., & Ort-  
839 meyer, M. (2006). Ice mass-balance buoys: A tool for measuring and attributing



- 840 changes in the thickness of the arctic sea ice cover. *Ann. Glaciol.*, *44*, 205–210.
- 841 Ricker, R., Hendricks, S., Helm, V., Skourup, H., & Davidson, M. (2014). Sen-  
842 sitivity of CryoSat-2 Arctic sea ice freeboard and thickness on radar-waveform  
843 interpretation. *The Cryosphere*, *8*(4), 1607–1622. doi: 10.5194/tc-8-1607-2014
- 844 Ricker, R., Hendricks, S., Kaleschke, L., Tian-Kunze, X., King, J., & Haas, C.  
845 (2017). A weekly Arctic sea-ice thickness data record from merged CryoSat-  
846 2 and SMOS satellite data. *The Cryosphere*, *11*, 1607–1623. doi: 10.5194/  
847 tc-11-1607-2017
- 848 Schulkes, R. (1995). A note on the evolution equations for the area fraction and  
849 the thickness of a floating ice cover. *Journal of Geophysical Research: Oceans*,  
850 *100*(C3), 5021–5024.
- 851 Schweiger, A., Lindsay, R., Zhang, J., Steele, M., Stern, H., & Kwok, R. (2011). Un-  
852 certainty in modeled Arctic sea ice volume. *J. Geophys. Res.*, *116*(9). doi: 10  
853 .1029/2011JC007084
- 854 Semtner Jr, A. J. (1976). A model for the thermodynamic growth of sea ice in  
855 numerical investigations of climate. *Journal of Physical Oceanography*, *6*(3), 379–  
856 389.
- 857 Serreze, M. C., Holland, M., & Stroeve, J. C. (2007). Perspectives on the Arctics  
858 shrinking sea-ice cover. *Science*, *315*, 1533–1536. doi: 10.1126/science.1139426
- 859 Shlyava, A., Buehner, M., Caya, A., Lemieux, J.-F., Smith, G. C., Roy, F., ...  
860 Carrieres, T. (2016). Towards ensemble data assimilation for the Environment  
861 Canada Regional Ice Prediction System. *Quart. J. Roy. Meteor. Soc.*, *142*, 1090–  
862 1099. doi: 10.1002/qj.2712
- 863 Shutts, G. (2005). A kinetic energy backscatter algorithm for use in ensemble pre-  
864 diction systems. *Quart. J. Roy. Meteor. Soc.*, *131*, 3079–3102. doi: 10.1256/qj.04  
865 .106
- 866 Smith, W. H. F., & Sandwell, D. T. (1997). Global seafloor topography from satel-  
867 lite altimetry and ship depth soundings. *Science*, *277*, 1957–1962. doi: 10.1126/  
868 science.277.5334.1956
- 869 Spreen, G., Kaleschke, L., & Heygster, G. (2008). Sea ice remote sensing us-  
870 ing AMSR-E 89-GHz channels. *J. Geophys. Res.*, *113*(2). doi: 10.1029/  
871 2005JC003384
- 872 Tian-Kunze, X., Kaleschke, L., Maaß, N., Mäkynen, M., Serra, N., Drusch, M., &

- 873 Krumpen, T. (2014). SMOS-derived thin sea ice thickness: Algorithm baseline,  
874 product specifications and initial verification. *The Cryosphere*, 8(3), 997–1018.  
875 doi: 10.5194/tc-8-997-2014
- 876 Ungermann, M., Tremblay, L. B., Martin, T., & Losch, M. (2017). Impact of the ice  
877 strength formulation on the performance of a sea ice thickness distribution model  
878 in the arctic. *Journal of Geophysical Research: Oceans*, 122(3), 2090–2107.
- 879 Wang, X., Key, J., Kwok, R., & Zhang, J. (2016). Comparison of Arctic sea ice  
880 thickness from satellites, aircraft, and PIOMAS data. *Remote Sens.*, 8(9). doi: 10  
881 .3390/rs8090713
- 882 Wingham, D. J., Francis, C. R., Baker, S., Bouzinac, C., Brockley, D., Cullen,  
883 R., . . . Wallis, D. W. (2006). Cryosat: A mission to determine the fluctua-  
884 tions in Earths land and marine ice fields. *Adv. Sp. Res.*, 37(4), 841–871. doi:  
885 10.1016/j.asr.2005.07.027
- 886 Xie, J., Counillon, F., Bertino, L., Tian-Kunze, X., & Kaleschke, L. (2016). Bene-  
887 fits of assimilating thin sea ice thickness from SMOS into the TOPAZ system. *The*  
888 *Cryosphere*, 10, 2745–2761. doi: 10.5194/tc-10-2745-2016
- 889 Yang, Q., Losa, S. N., Losch, M., Jung, T., & Nerger, L. (2015a). The role of at-  
890 mospheric uncertainty in arctic summer sea ice data assimilation and prediction.  
891 *Quarterly Journal of the Royal Meteorological Society*, 141(691), 2314–2323.
- 892 Yang, Q., Losa, S. N., Losch, M., Liu, J., Zhang, Z., Nerger, L., & Yang, H. (2015b).  
893 Assimilating summer sea-ice concentration into a coupled ice–ocean model using a  
894 lseik filter. *Annals of Glaciology*, 56(69), 38–44.
- 895 Yang, Q., Losa, S. N., Losch, M., Tian-Kunze, X., Nerger, L., Liu, J., . . . Zhang,  
896 Z. (2014). Assimilating SMOS sea ice thickness into a coupled ice-ocean  
897 model using a local SEIK filter. *J. Geophys. Res.*, 119(10), 6680–6692. doi:  
898 10.1002/2014JC009963
- 899 Yang, Q., Losch, M., Losa, S. N., Jung, T., Nerger, L., & Lavergne, T. (2016a). Brief  
900 communication: The challenge and benefit of using sea ice concentration satellite  
901 data products with uncertainty estimates in summer sea ice data assimilation.  
902 *The Cryosphere*, 10(2), 761–774. doi: 10.5194/tc-10-761-2016
- 903 Yang, Q., Losch, M., Loza, S., Jung, T., & Nerger, L. (2016b). Taking into account  
904 atmospheric uncertainty improves sequential assimilation of SMOS sea ice thick-  
905 ness data in an ice-ocean model. *J. Atmos. Oceanic Technol.*, 33, 397–407. doi:

906 10.1175/JTECH-D-15-0176.1

907 Zhang, J., & Hibler, W. D., III. (1997). On an efficient numerical method for mod-  
908 eling sea ice dynamics. *J. Geophys. Res.*, *102*(C4), 8691–8702. doi: 10.1029/  
909 96JC03744

910 Zhang, J., Hibler, W. D., III, Steele, M., & Rothrock, D. A. (1998). Arctic ice-ocean  
911 modeling with and without climate restoring. , *28*(2), 191–217.

912 Zhang, J., & Rothrock, D. A. (2003). Modeling global sea ice with a thickness  
913 and enthalpy distribution model in generalized curvilinear coordinates. , *131*(5),  
914 845–861. doi: 10.1175/1520-0493(2003)131<0845:MGSIIWA>2.0.CO;2